I&EC research
Industrial & Engineering Chemistry Research

pubs.acs.org/IECR
Article

Mixing of Immiscible Polymers in the Solid State

Iurii Vozniak,* Roman Kulagin, Victor Beloshenko, Ramin Hosseinnezhad, Artur Rozanski, Andrzej Galeski, Salim-Ramy Merouani, and Bogdan Savchenko

Cite This: *Ind. Eng. Chem. Res.* 2025, 64, 7739−7750

ABSTRACT: Traditionally, both miscible and immiscible polymers are mixed in solution and melt. In this work, the possibility of mixing immiscible polymers in the solid phase is studied on the example of three pairs of thermodynamically incompatible polymers—ABS/PET, PETG/PBT, PLA/PBT. It is shown that mixing in the solid phase is possible under the conditions of the combined effect of high pressure and shear deformation. High-pressure torsion (HPT) was chosen as the mixing technique. The values of critical accumulated shear strain, which allow the transition from immiscible to miscible blend, were determined. It was found that a higher torsion speed contributes to a faster transition and a higher pressure to a higher degree of convergence of the mixed phases. The homogeneous mixed structure formed is stable above its glass transition or melting temperature after short-term annealing.

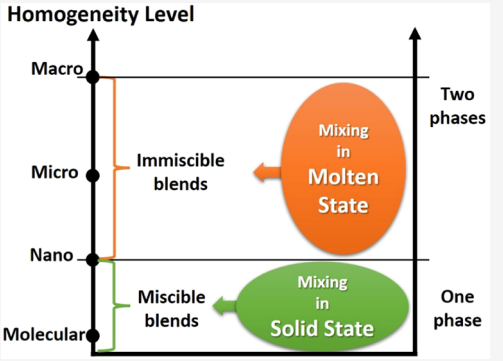

INTRODUCTION

Homogeneous mixing of thermodynamically incompatible polymers is of critical importance in chemistry, materials, and engineering. Compatibilization of macromolecules is used commercially to produce new materials with tailored properties. However, unlike low molecular weight compounds, the mixing entropy of macromolecules is inherently very low and the mixing enthalpy of polymer pairs is significantly positive. Therefore, mixing two or more polymers in most cases results in phase separation at the macroscopic level. This fatal problem represents a significant obstacle to the preparation of many scientifically and technologically relevant homogeneous blends.

Recently, several approaches have been proposed to promote miscibility, e.g., the addition of tailored block or graft copolymers or the addition of reactive polymers,[1,2] the addition of multifunctional copolymers as impact modifiers or the addition of cosolvents;[3] by ionic interaction and by irradiation or electron beam (in combination with or without coagents);[4] by the simultaneous formation and coalescence of common crystalline inclusion compounds between host cyclodextrins and two or more guest polymers.[5] Most recently, new approaches have attracted interest: compatibilization by addition of targeted nanoparticles and nanoplatelets and their localization at the polymer/polymer interface;[6−10] addition of gradient copolymers;[11] mixing by supramolecular complexation, porous coordination polymers, fluid interfaces;[12−16] by synthesis of an interpenetrating dual network or by thermomechanically forcing the interpenetration of the double network,[17,18] solid-state pulverization[19−21] and mixing by forced assembly.[22−24]

All of these approaches can be divided into those based on (i) compatibilization, which theoretically leads to a reduction in interfacial tension and/or steric hindrances to coalescence and an improvement in adhesion between the phases in contact, and (ii) those based on the creation of dynamic bonds, i.e., polymer units that can reversibly change their composition. The resulting blends themselves can be conditionally divided into mechanically miscible polymer blends (prepared by melt mixing of the polymers or by using coordination templates) or mechanochemically miscible polymer blends (when free radicals formed during processing react with the polymers) and chemically miscible polymer blends (prepared by in situ polymerization and cross-linking of the constituent polymers). It should be noted that the polymer blends commercially available are almost exclusively mechanical polymer blends.

While a considerable body of knowledge has been accumulated with respect to the mixing of immiscible polymers in solution or melt,[25−28] mixing of polymers in the solid state has been hardly explored. However, it should be mentioned that some aspects of mixing materials in the solid state, i.e., the formation of solid solutions, have been studied for immiscible metals.[29−33] Two of the most important techniques suitable for the synthesis of nonequilibrium phases in immiscible alloy

Received: January 21, 2025
Revised: March 28, 2025
Accepted: March 28, 2025
Published: April 3, 2025

https://doi.org/10.1021/acs.iecr.5c00328
Ind. Eng. Chem. Res. 2025, 64, 7739−7750

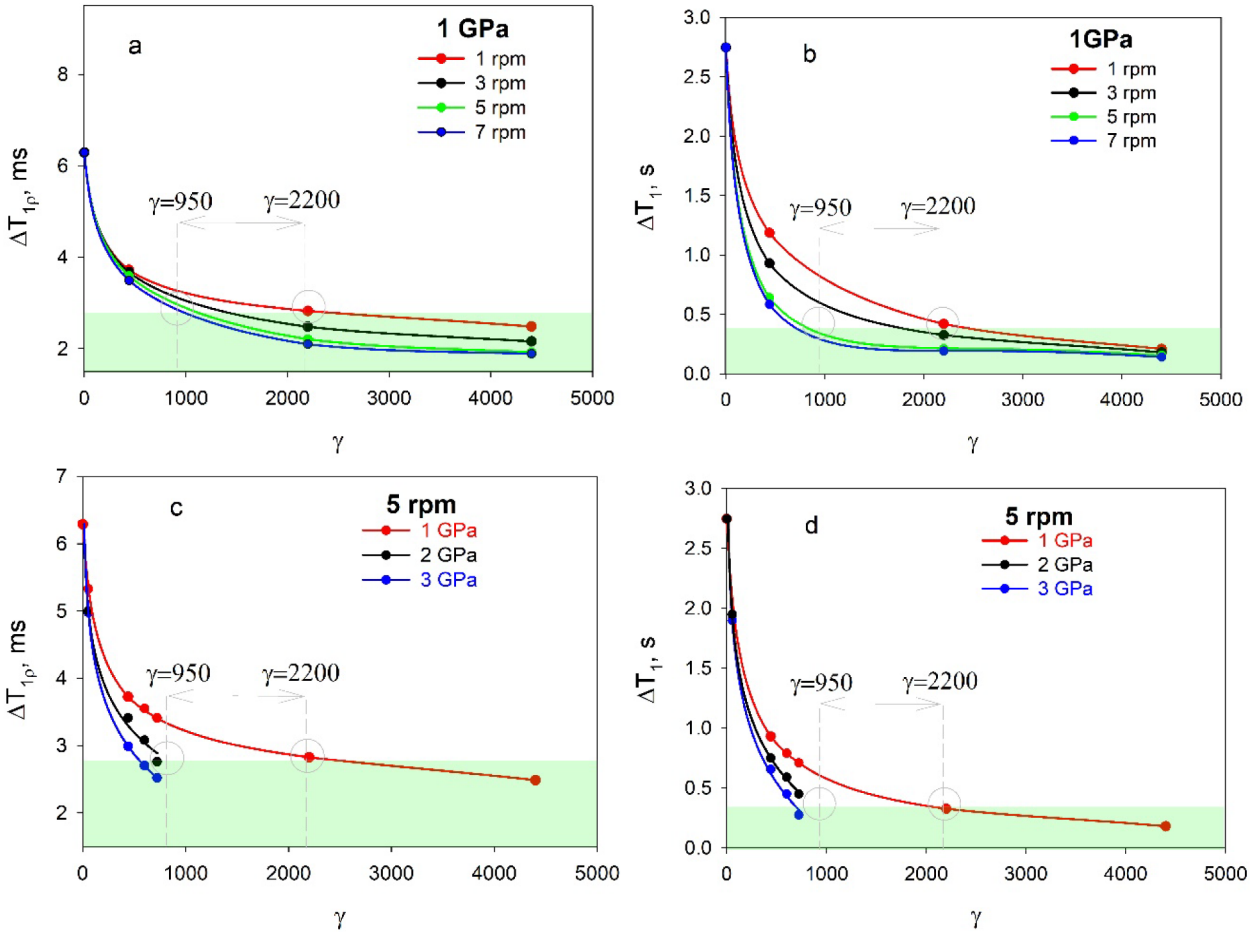

Figure 1. Solid-state NMR analysis of ABS/PET blend. Effect of accumulated shear strain γ and torsion speed on ΔT_1 and $\Delta T_{1\rho}$. The T_1 and $T_{1\rho}$ recovery curves for the ABS/PET blends are shown in Figures S1 and S2.

systems are mechanical alloying, which consists of repeated cold welding, fracturing, and rewelding of powder particles in a high-energy ball mill,[34] and high-pressure torsion (HPT), in which thin sheets of different metals are stacked on top of each other and subjected to high-pressure torsion.[35] All these techniques can produce different types of metastable phases, e.g., supersaturated solid solutions, crystalline and quasi-crystalline intermediate phases, and also amorphous phases. HPT, in particular, has the unique ability to cause phase dissolution,[36,37] disorder of ordered phases,[38] and amorphization of crystalline phases[39] or crystallization of nanocrystals in amorphous matrices.[40] Unlike mechanical alloying, which typically does not facilitate phase dissolution, HPT can dissolve phases in the solid state due to the high pressure and significant deformation it applies. This makes HPT an attractive method for mixing incompatible polymers, as it bypasses the constraints of traditional phase diagrams that apply to liquid-phase methods.

Furthermore, in contrast to chemical compatibilization approaches, which rely on the use of potentially harmful additives or coagents, HPT is an environmentally friendly technique. It does not require any chemical substances and instead achieves polymer blending purely through mechanical processes, making it a more sustainable and eco-friendly alternative for producing polymer blends.

It is also worth noting that previous studies have explored the possibility of mixing immiscible polymer blends using HPT.[41−43] However, Zhorin et al.[41] and Yenikolopyan et al.[42,43] have reached contradictory conclusions regarding the feasibility of mixing thermodynamically incompatible polymers in this way. These differences may arise from variations in experimental conditions, such as pressure, strain, and torsion speed, all of which can significantly influence the success of HPT in blending incompatible polymers.

In this work, we investigate the possibility of mixing immiscible polymers in the solid state using HPT. Three polymer systems were selected, namely ABS/PET, PETG/PBT and PBT/PLA, which are normally immiscible using standard solution and melt mixing methods. Solid-state NMR, DSC, TGA, TEM were selected to study the homogeneity of the blends.

RESULTS AND DISCUSSION

It is known that in immiscible polymer blends characterized by phase separation, each phase has a different characteristic 1H spin−lattice relaxation time in the laboratory frame (T_1). In miscible polymer blends characterized by nanoscale phase mixing, the relaxation times for all polymer phases that make up the blend are relatively close to each other. Moreover, the 1H spin−lattice relaxation times determined in the rotating frame ($T_{1\rho}$) characterize the homogeneity of the polymer blend on the nanometer scale. Therefore, for the case of a two-phase polymer system, the quantities $\Delta T_1 = T_{1I}$ (phase I) − T_{1II} (phase II) and $\Delta T_{1\rho} = T_{1\rho I}$ (phase I) − $T_{1\rho II}$ (phase II) can

https://doi.org/10.1021/acs.iecr.5c00328
Ind. Eng. Chem. Res. 2025, 64, 7739−7750

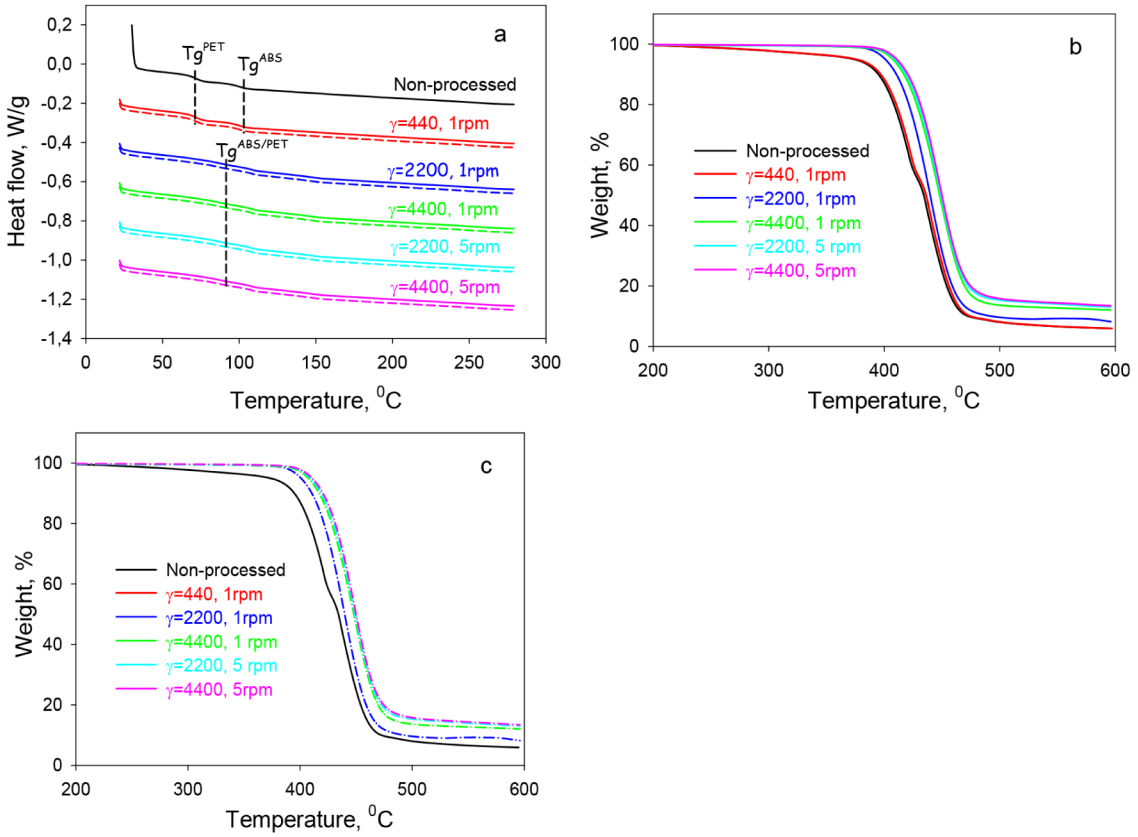

Figure 2. Thermal analysis of ABS/PET blends. DSC (a) and TGA (b,c) thermograms of ABS/PET blends processed at different accumulated strains and torsion speeds: first heat (solid lines) and second heat/annealing (dashed lines), p = 1 GPa. Corresponding DSC and TGA data for blends processed at 2 and 3 GPa are shown in Figure S3.

be used to characterize the dynamics of the transition from an immiscible to a miscible blend. The more homogeneous the polymer blend becomes and the more intimate the contact between the phases, the more the values of T_1 and $T_{1\rho}$ for each of the phases approach each other and the smaller the corresponding values of ΔT_1 and $\Delta T_{1\rho}$ are.

Figure 1a,b shows the dependencies of ΔT_1 and $\Delta T_{1\rho}$ on the value of accumulated shear strain γ for the ABS/PET blends processed at different torsion speeds. It can be seen that the initial ABS/PET blend is characterized by large ΔT_1 and $\Delta T_{1\rho}$ values, which is typical of immiscible blends where the relaxation times of the individual phases differ significantly. With increasing accumulated strain, the values of ΔT_1 and $\Delta T_{1\rho}$ decrease, indicating the occurrence of mixing and homogenization processes. The values of ΔT_1 and $\Delta T_{1\rho}$ decrease progressively with strain up to about γ = 440, but then level off as strain continues to increase. The crossover points observed near γ = 950−2200 could correspond to the transition from an immiscible to a miscible blend, and the presence of a plateau in the range γ = 2200−4400 indicates the formation of a saturation state in the blend. The torsion speed influences the dynamics of this transition. As the torsion speed increases to 3 and 5 rpm, the decrease in ΔT_1 and $\Delta T_{1\rho}$ becomes more pronounced and less smooth compared to the 1 rpm case. However, further increasing the torsion speed to 7 rpm does not lead to a more significant reduction in ΔT_1 and $\Delta T_{1\rho}$ At 7 rpm, the changes in ΔT_1 and $\Delta T_{1\rho}$ are minimal compared to 5 rpm. It is also important to note that the absence of a subsequent increase in the values of ΔT_1 and $\Delta T_{1\rho}$ at γ > 2200 proves the stability of the blends obtained by HPT and the absence of phase segregation.

The results shown in Figure 1a,b correspond to the case of an applied pressure of 1 GPa. Increasing the pressure to 2 and 3 GPa causes a significant shift of the crossover points to lower values of accumulated shear strain (Figure 1c,d). For ABS/PET blends, which are processed at 3 GPa, 5 rpm already at γ = 720, show ΔT_1 = 0.298 s and $\Delta T_{1\rho}$ = 2.505 ms. It can be assumed that the higher pressure, at which the solid phase mixing occurs, promotes a greater degree of phase convergence in the HPT-processed blend. It should be noted that, unlike torsion speed, the applied pressure does not exhibit a saturation effect as it increases. Instead, the values of ΔT_1 and $\Delta T_{1\rho}$ continue to decrease with rising pressure. Unfortunately, further increasing the pressure to 5−7 GPa, or accumulating high strain values at 2 and 3 GPa, is currently technically impossible due to probability of ″jamming″ or welding effects in the anvils. However, it should be noted that higher pressures will help maintain the polymers in the solid phase, preventing the decaying of thin, deformed polymer layers and their subsequent coalescence into larger structures, as seen in polymer blend melts. This is because an increase in pressure would raise the transition temperature by approximately 2−4 °C for every 100 MPa.

The DSC (Figure 2a) and TGA (Figure 2b) results are consistent with the solid-state NMR results and confirm the HPT-induced transition from an immiscible to a miscible ABS/PET blend. It should be emphasized that the NMR results show homogeneous mixing of the phases at the nanoscale, while DSC and TGA indicate homogeneous mixing

https://doi.org/10.1021/acs.iecr.5c00328
Ind. Eng. Chem. Res. 2025, 64, 7739−7750

at the microscale and are not sensitive to possible heterogeneity of phase mixing at the nanoscale. The presence of two distinct glass transition temperatures at 75 °C and 108 °C, which are related to the processes of α-transition of ABS and PET, respectively, in the DSC curves and two decomposition steps at temperatures of 230−425 °C and 425−505 °C (T_d) in the TGA curves, indicates the presence of two immiscible phases in the case of the initial ABS/PET blend. In contrast, a single wide α-transition at an intermediate temperature between the glass transition temperatures of PET and ABS and a uniform decomposition of 375−505 °C in the case of the HPT-processed blends with $\gamma > 2200$ indicates the formation of PET and ABS phases that devitrify and decompose together, i.e., the formation of a well-mixed single amorphous ABS/PET phase at the microscale. Since no well-defined glass transition is observed, but a flat heat capacity response occurs, the position of the hypothetical glass transition for miscible systems is marked in Figure 2. It can be seen that the accumulated strain and torsion speed have no effect on the glass transition for miscible ABS/PET blends. Nevertheless, there is a clear tendency for the onset decomposition temperature to increase with increasing accumulated shear strain.

The results obtained are not only typical for the system ABS/PET, but are also repeated for other systems investigated: PETG/PBT and PLA/PBT. The solid-state NMR, DSC and TGA results for these systems are shown in Table 1. The data

Table 1. Characteristics of the Initial and HPT-Processed Blends (5 rpm)

Process parameters	ΔT_1 (s)	$\Delta T_{1\rho}$ (ms)	T_g (°C)	T_d (°C)
PLA/PBT				
initial	1.79	27.93	67/57	315−400/400−450
γ = 2200, 1 GPa	1.09	2.91	62	335−450
γ = 440, 2 GPa	0.96	2.07	62	337−450
γ = 440, 3 GPa	0.32	0.98	62	337−451
PETG/PBT				
initial	1.91	1.66	77/58	350−420/420−475
γ = 2200, 1 GPa	0.75	1.82	68	370−420
γ = 440, 2 GPa	0.40	0.14	68	372−420
γ = 440, 3 GPa	0.09	0.09	68	372−420

in Table 1 show the following trends: for all polymer pairs (PLA/PBT, PETG/PBT), the initial blends are clearly phase segregated, with high ΔT_1 and $\Delta T_{1\rho}$ values. After HPT processing, the values of ΔT_1 and $\Delta T_{1\rho}$ significantly decrease, indicating that phase mixing has occurred. Specifically, at γ = 2200 and pressures of 1, 2, and 3 GPa, the blends approach a homogeneous state, with minimal phase separation. Additionally, the glass transition temperatures and decomposition temperatures also indicate the shift from a two-phase to a single-phase system, confirming the effect of HPT processing on phase homogeneity.

The corresponding DSC, TGA and solid state NMR data are shown in Figures S4 and S5.

Figure 3 shows the TEM images of the initial and HPT-processed (γ =2200, 5 rpm, 1 GPa) ABS/PET, PETG/PBT blends as an example. The initial blends are characterized by a macroscopically separated structure with ABS/PET and PETG/PBT layers. For the ABS/PET blends, as shown in Figure 3a,b, the polymer components remain phase-separated at the macro scale. Similarly, the PETG/PBT blends, represented in Figure 3e,f, also exhibit a distinct layered structure in their initial state. However, after HPT processing, the HPT-processed ABS/PET blends, shown in Figure 3c,d, shows no layered structures, and the contrast between the polymer components disappears at the nanometer scale, indicating a homogeneous mix. The PETG/PBT blends (Figure 3g,h) follow a similar trend; after processing, the layered structure is no longer visible, and the blend becomes homogeneous at the nanoscale. This observation suggests that solid-phase mixing has effectively broken down the initial phase-separated structure in both the ABS/PET and PETG/PBT blends.

One possible mechanism for solid phase mixing is the mechanical thinning of the polymer layers in the shear direction to nanoscale sizes. To verify that solid-phase mixing involves stirring the polymer layers, carbon black particles were added to the initial layers of one of the polymers, PET (black inclusions in Figure 3a−d). It can be seen that the filler was evenly distributed at nanometer scale over the entire volume of the blend after solid-state mixing, indicating stirring of the polymer layers down to the nanoscale.

Following these observations, Figure 4 presents a phase diagram showing the transition from immiscible to miscible blends for the systems studied under solid-phase mixing conditions. This phase diagram is constructed based on the accumulated shear strain (γ) and pressure applied during HPT processing. It highlights the critical parameters—pressure and accumulated shear strain—that dictate the efficiency of homogenization in the polymer blends. The phase boundary, separating immiscible two-phase systems from homogeneous single-phase systems, is determined using transmission electron microscopy (TEM) data.

The diagram illustrates that as the accumulated strain increases, the polymer blends gradually transition from a two-phase system, where the polymer components remain phase-separated, to a single-phase system, where the components are intimately mixed at the nanoscale. Higher pressures accelerate this transition, playing a significant role in promoting phase convergence. Additionally, a faster transition to a miscible state is observed at higher torsion speeds, demonstrating the dynamic interplay between shear deformation and pressure during the blending process.

The presence of a stirring process is also confirmed by the pole figure data (Figure 5). The initial PETG/PBT blend exhibited a layered structure, with alternating PETG and PBT layers formed by 3D printing. The broad concentration of the (110) pole near the center indicates a weak alignment of the polymer chains parallel to the deposition plane during 3D printing. In contrast, the pole figure of the (110) plane for the HPT-processed PETG/PBT blend shows a significantly higher pole density, evenly distributed in a circle between the central and peripheral regions. This texture suggests that the polymer chains are oriented at approximately 45° relative to the shear deformation plane. A similar pattern for the (110) plane was observed in the PLA/PBT system (Figure S6). These findings indicate that not only do the polymer layers become thinner, but they also undergo dynamic movement, likely driven by Taylor vortex flow.[44]

The blends produced by solid-phase mixing are highly stable. No significant phase separation is observed after heating above the melting temperatures or annealing above the glass transition temperatures for a short period (120 °C for 1 h for ABS/PET, and 230 °C for 1 h for PETG/PBT and PLA/

https://doi.org/10.1021/acs.iecr.5c00328
Ind. Eng. Chem. Res. 2025, 64, 7739−7750

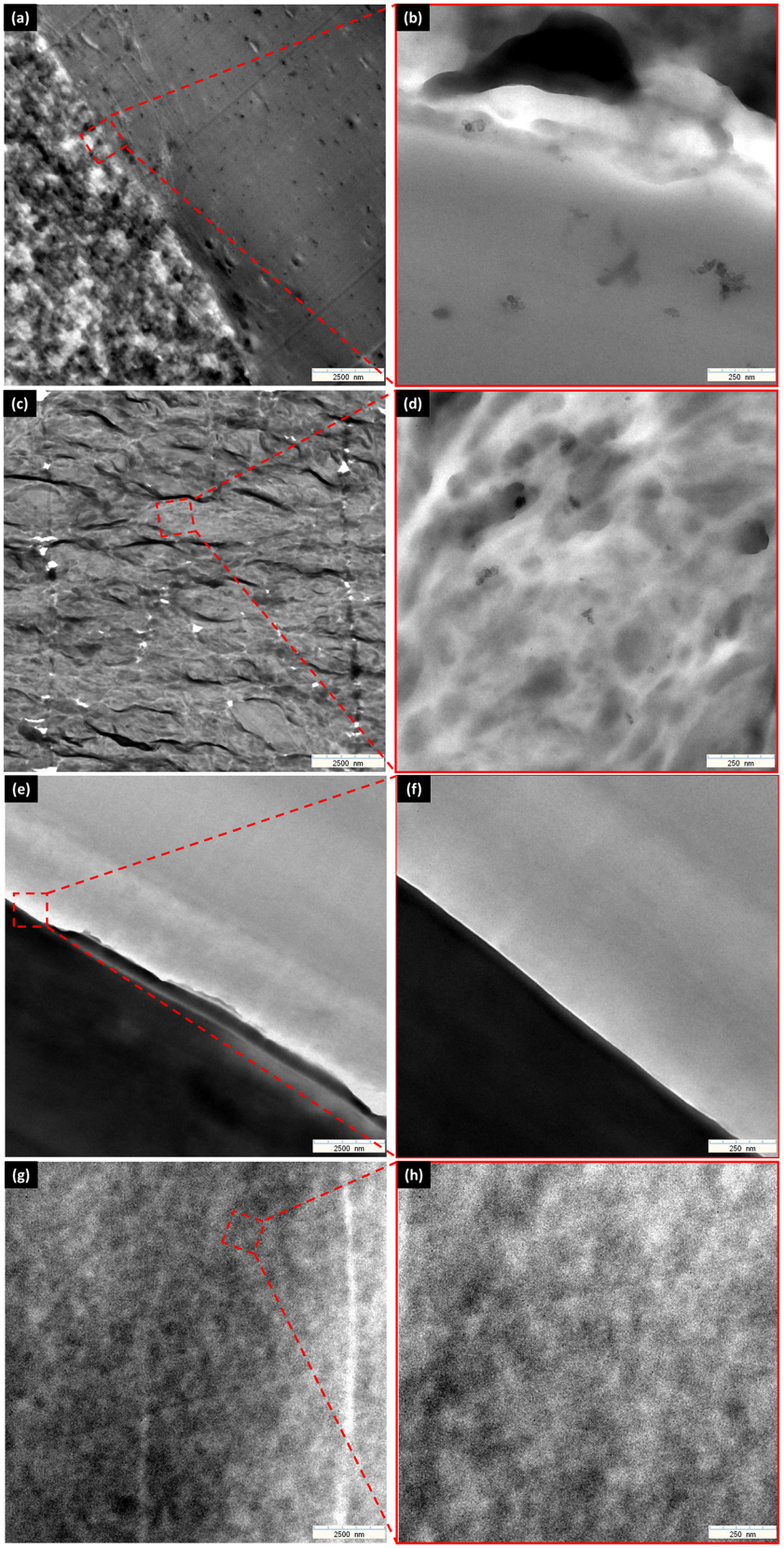

Figure 3. Morphology of ABS/PET and PETG/PBT blends. TEM images of ABS/PET (initial (a,b), HPT-processed (c,d)) and PETG/PBT (initial (e,f), HPT-processed (g,h)) blends.

PBT). As shown in Figures 2 and 6, for HPT-processed blends, the DSC curves from the second heating cycle show only a single glass transition, and the TGA curves exhibit uniform decomposition. Extended heating times (5 h, 10 h, 15 h, 24 h, 48 h) above the melting or glass transition temperatures also did not result in phase separation. However, for crystalline

https://doi.org/10.1021/acs.iecr.5c00328
Ind. Eng. Chem. Res. 2025, 64, 7739−7750

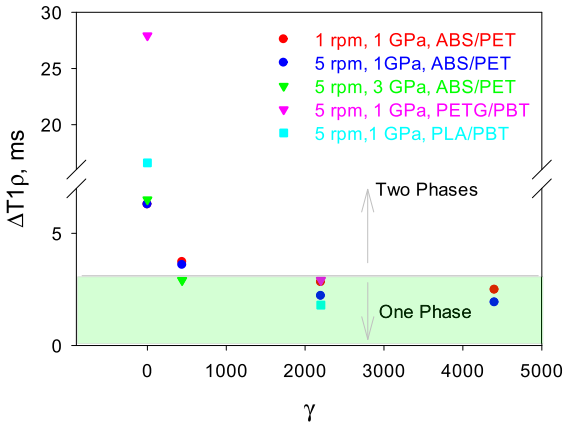

Figure 4. A phase diagram for the systems studied. The line on the phase diagram separating two-phase from one phase systems are obtained based on TEM data.

polymers, extended heating led to a decrease in crystallinity. More defective crystalline structures were observed in polymers with lower melting points. This is likely because the annealing temperatures were set above the melting point of the higher-melting polymer, which turned out to be too high for the lower-melting polymers. Crystallization temperatures remained unchanged during annealing (Figure S7).

The reason why the HPT-processed blends are not affected in their intimacy of mixing by the heating and annealing conditions described above, even though both polymers of the constituent blend should have sufficient mobility for phase separation under the action of a thermodynamic driving force given by the inherent incompatibility, could be the following. The unfavorable heat of mixing is known to be compensated by the entropy of the intimately mixed blend. It is likely that HPT leads to an increase in the mixing entropy of the macromolecules, which more effectively prevents phase separation. The results of the WAXS study support the latter assumption (Figure 7). It can be seen that both an increase in pressure and an increase in accumulated strain lead to an increase in the intensity of the amorphous halo peak, which is directly proportional to the fluctuation-free volume in the amorphous phase and is an indicator of the degree of disorder in the glassy state.[45,46] According to existing concepts, the amorphous structure in polymers is heterogeneous and consists of more densely packed (with local order) and less densely packed (without local order) components.[46,47] Local order is a disruption (interruption) of total disorder. Accordingly, the absence of local order represents total disorder, as in the "felt" model proposed by Flory.[48,49] Reduction of the fraction of a densely packed component (with local order), its destruction (disordering) under the action of HPT, can facilitate easier movement of macromolecules of mixed polymers and cause an increase in the mixing entropy of macromolecules. HPT also contributes to the destruction of the crystalline phase, i.e., it also causes the transition from order to disorder. Changing the torsion speed has practically no effect on the intensity of the amorphous peaks (Figure 7).

It should be noted, however, that the net driving force for the separation of intimately mixed but generally incompatible polymer pairs into separate phases is relatively small and takes time to achieve. It is expected that the stability of such systems will deteriorate and phase separation may occur over prolonged annealing.

The transition from an immiscible to a miscible polymer blend morphology leads to significant improvements in both stiffness and strength. The results of uniaxial tensile tests for both melt-mixed and HPT-processed blends are summarized in Table 2, with the corresponding stress−strain curves shown in Figure S9. Compared to the melt-mixed blends, the HPT-processed samples exhibit a 37% (ABS/PET), 43% (PETG/PBT), and 116% (ABS/PET) increase in the modulus of elasticity, and a 46% (PETG/PBT) and 37% (PLA/PBT, ABS/PET) increase in yield strength. Higher pressure results in a higher elastic modulus and yield strength, even at lower accumulated strain levels. The increased yield strength and modulus of elasticity in the HPT-processed blends are likely due to denser molecular packing and stronger interactions between the blend components at the interface. Although the plastic properties did not improve compared to the melt mixed samples, they remained consistent, suggesting that the high-

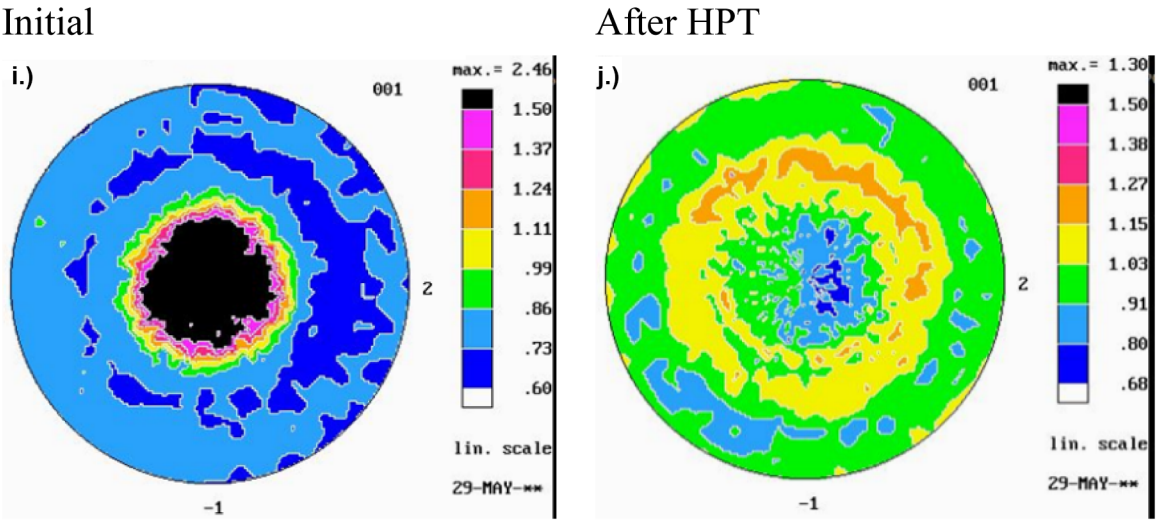

Figure 5. Texture analysis of PETG/PBT blends. Normalized pole figures of the (110) crystallographic plane determined for initial and HPT processes PETG/PBT blends (γ = 2200, 5 rpm, 1 GPa).

https://doi.org/10.1021/acs.iecr.5c00328
Ind. Eng. Chem. Res. 2025, 64, 7739−7750

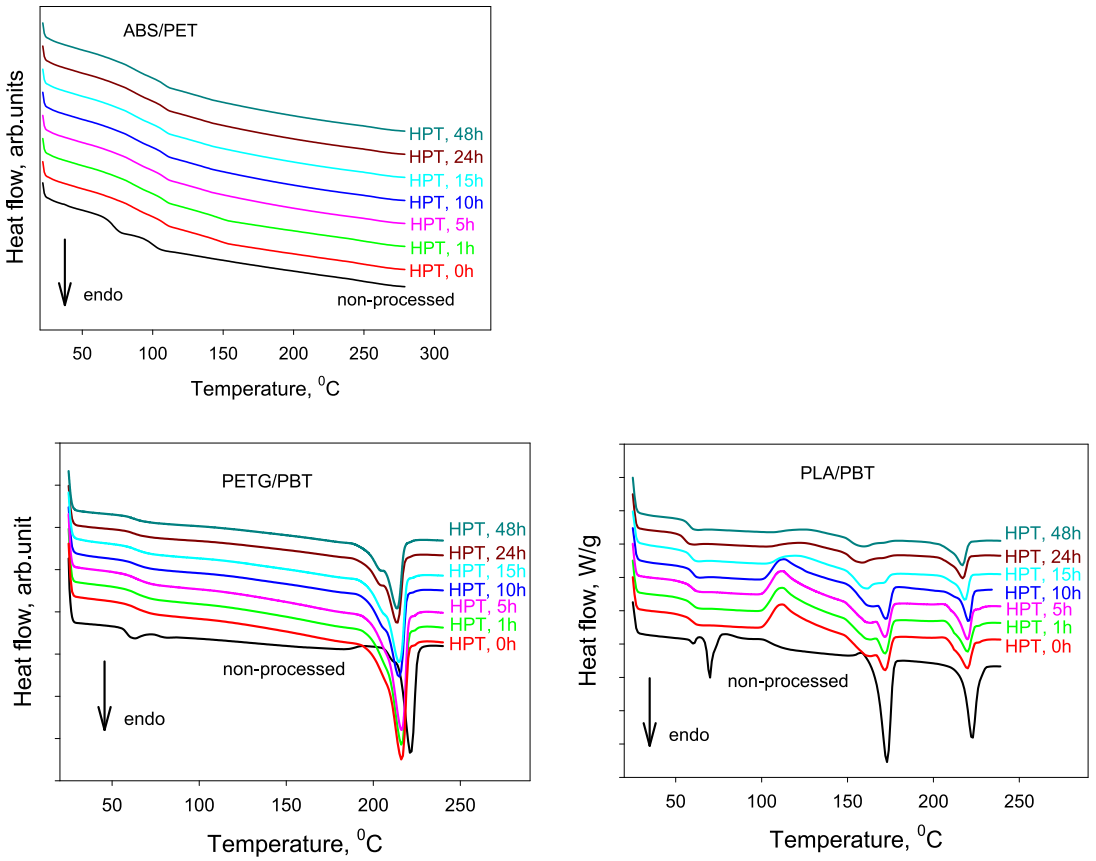

Figure 6. Thermal analysis of ABS/PET, PETG/PBT and PLA/PBT blends. Effect of heating HPT-processed samples above the melting temperatures or annealing above the glass transition temperatures (120 °C for ABS/PET, and 230 °C for PETG/PBT and PLA/PBT) on their thermal behavior.

pressure treatment in HPT effectively heals damage caused by significant deformation.

CONCLUSION

We have demonstrated an alternative strategy for the preparation of polymer blends that are intimately mixed at the nanometer scale. A variety of immiscible polymer pairs that traditionally do not mix in solution or melt could be homogeneously mixed by subjecting the material to high pressure and shear deformation in solid phase. The mechanical method of homogenizing polymer blends speaks to the prospects for its commercialization. For the studied systems ABS/PET, PETG/PBT, PETG/PLA, the transition from immiscible to miscible blend was observed as a result of HPT at an accumulated shear strain γ = 950−2200, the value of which was adjusted by the torsion speed. More homogeneous blends were obtained at higher pressures. A possible mechanism for the mixing of immiscible polymers under the conditions of high pressure and shear deformation is the codeformation of mixed polymer phases, which is accompanied by a gradual decrease in the thickness of the layers of mixed polymers down to nanosizes, as well as the destruction of the long- and short-range order in the crystalline and amorphous phases of mixed polymers, respectively. These processes lead to an increase in the mixing entropy of the macromolecules, which has a favorable effect on the stability of the obtained mixtures. Blends mixed in the solid phase maintain the stability of the homogeneous structure formed during both short-term and long-term annealing at temperatures above their melting point or glass transition temperature.

MATERIALS AND METHODS

High Pressure Torsion Setup. In HPT mixing, a disc-shaped specimens of different polymers are placed between two anvils, both of which have a cylindrical cavity with a depth slightly less than the thickness of the specimen. During mixing, one of the HPT anvils is fixed while the other rotates. Ideally, polymers are mixed through the plastic deformation by simple shear. In this case, the different initial phases in a binary or multiphase system are stretched in the shear direction and their thickness is continuously reduced. In order to reach a state of saturation or equilibrium in a multiphase system, i.e., that the microstructural features of the sample do not change further during the ongoing HPT deformation, the applied shear strain must be sufficient to reduce the thicknesses of the sheared phases down to the nanometer range.

Layered polymer samples in the form of a disc with a diameter of 13 mm and a thickness of 3 mm were used. The samples were processed on a self-made HPT installation (W. Klement GmbH, Lang, Austria). Standard semiconstrained anvils Figure 8 with a diameter of 13 mm and a thickness of 1 mm were used. All experiments were carried out according to the following scheme. First, the sample was unloaded until the required pressure level was reached. In this work, pressure in the range of 1−3 GPa was applied during the mixing process. Then one of the anvils was brought into rotation with a given angular velocity (torsion speed), while the regulator automati-

https://doi.org/10.1021/acs.iecr.5c00328
Ind. Eng. Chem. Res. 2025, 64, 7739−7750

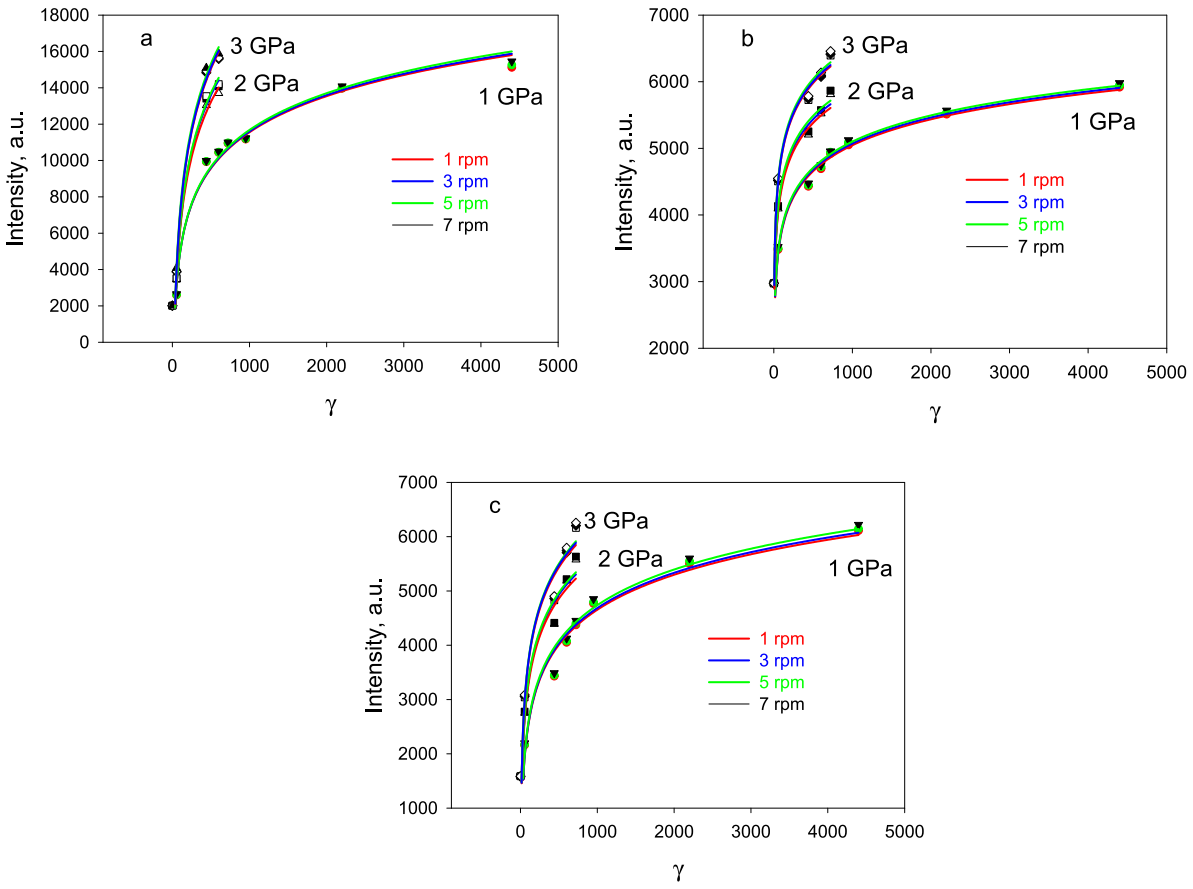

Figure 7. Order−disorder transition analysis in the studied blends. Dependence of the amorphous halo peak intensity on pressure, accumulated strain, and torsion speed for ABS/PET (a), PLA/PBT (b), and PETG/PBT (c). Corresponding X-ray diffraction patterns are shown in Figure S8.

Table 2. Mechanical Properties of the Initial and HPT-Processed Blends

	Modulus of Elasticity (MPa)		Yield stress (MPa)		Yield strain (%)	
Blend	Nonprocessed	After HPT	Nonprocessed	After HPT	Nonprocessed	After HPT
ABS/PET	1084 ± 150	2300 ± 207[a]	19.3 ± 1.5	23.4 ± 1.2[a]	2.20 ± 0.15	1.17 ± 0.10[a]
		2325 ± 190[b]		24.2 ± 1.3[b]		1.18 ± 0.10[b]
		2342 ± 175[c]		26.6 ± 1.2[c]		1.18 ± 0.10[c]
PLA/PBT	1662 ± 249	2242 ± 267[a]	30.0 ± 1.5	36.1 ± 1.3[a]	1.80 ± 0.05	1.94 ± 0.06[a]
		2370 ± 200[b]		39.2 ± 1.2[b]		1.91 ± 0.08[b]
		2390 ± 210[c]		41.2 ± 1.3[c]		1.93 ± 0.07[c]
PETG/PBT	1676 ± 201	2173 ± 213[a]	25.3 ± 1.4	30.4 ± 1.1[a]	1.88 ± 0.09	1.83 ± 0.10[a]
		2260 ± 220[b]		34.9 ± 1.2[b]		1.83 ± 0.10[b]
		2295 ± 200[c]		37.1 ± 1.3[c]		1.84 ± 0.09[c]

[a]γ = 2200, 5 rpm, 1 GPa. [b]γ = 440, 5 rpm, 2 GPa. [c]γ = 440, 5 rpm, 3 GPa.

cally maintained the required pressure level throughout the whole deformation. Torsion speeds were 1, 3, 5, and 7 rpm. All experiments were carried out at ambient temperature.

Shear strain in the HPT method was calculated according to the equation:[50]

$$\gamma = \frac{2\pi Nr}{h}$$

where γ is the shear strain, r is the distance from the disc center, N is the number of anvil rotations and h is the thickness of the disc. This equation suggests that extremely large strains can be achieved in this method by increasing the number of rotations. Assuming that two phases with an initial size of d_0 are subjected to ultrahigh plastic deformation, their thickness is reduced geometrically based on the following equation, assuming that the two phases deform in an ideal manner:[51]

$$d = d_0/\gamma$$

This equation, which is valid only at large shear strains, states that the thickness of the two phases with a size of 1 μm (a normal size in many materials) can be reduced to the nanometer range when subjected to a shear strain of 1,000.

Materials. Acrylonitrile butadiene styrene copolymer (ABS; Terluran GP-22), having melt flow index, MFI = 18 g/10 min (220 °C/10 kg, ASTM D1238), poly(ethylene terephthalate) (PET; EKOPET 80BB) with MFI = 16 g/10 min (220 °C/2.16 kg, ASTM D1238) in an amorphous state, polylactide (PLA; Luminy L175), having melt flow index, MFI

https://doi.org/10.1021/acs.iecr.5c00328
Ind. Eng. Chem. Res. 2025, 64, 7739−7750

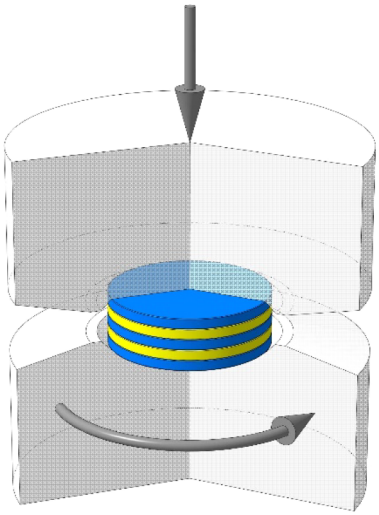

Figure 8. Schematics of high-pressure torsion of a layered polymer specimen.

= 8 g/10 min (210 °C/10 kg, ASTM D1238), polybutylene terephthalate (PBT; Crastin 6129 NC010) with MFI = 8 g/10 min (250 °C/2.16 kg, ASTM D1238) and glycol-modified polyethylene terephthalate (PET-G; Eastar Copolyester 6763) with MFI = 8 g/10 min (265 °C/2.16 kg, ASTM D1238) were used in the experiments.

Sample Preparation. An initial blend with 50 wt %/50 wt % polymer components was produced on the Flashforge Creator Pro three-dimensional printer by alternately depositing layers of blended polymers. A detailed description of the 3D printing process can be found elsewhere.[52]

Characterization. The X-ray measurements were performed with a Aeris XRD diffractometer (Malvern Panalytical) operating at 40 kV and 7.5 mA. The material before and after HPT were grinded for XRD measurements in order to randomize the polymer crystal orientation.

The texture of initial and HPT-processed samples was also studied in detail using the X-ray pole figure technique (for an overview of this technique, see e.g. 53. The WAXS system consisted of a computer-controlled pole figure device in combination with a wide-angle goniometer coupled to a closed tube source of Ni-filtered CuK radiation (λ = 0.154 nm) operating at 50 kV and 40 mA (Panalytical B.V., Almelo, The Netherlands). The samples have the shape of approximately 2 mm thick discs. The pole figures of the (001) plane of PBT were chosen because this plane is parallel to the chain axis and is the main plane for crystallographic sliding of polymer crystals.[54] Therefore, the appearance of a crystalline texture (elevated pole density) would indicate the presence of vortices and the orientation of most polymer crystals after solid phase mixing.

Diffraction intensity data were collected at a fixed Bragg angle corresponding to the position of the diffraction peak of the plane of interest ($2\Theta = 9°$[54]), while the pole (tilt) angle and the azimuth angle of the sample holder were changed stepwise (in 5 steps) in the ranges of 0−90° and 0−360°, respectively. To create complete pole figures, it was necessary to collect data in both transmission and reflection modes. The joint angle at which the data from the transmission and reflection modes were combined was 50°. The pole figures were calculated from the collected data after all necessary corrections for background scattering, sample absorption and instrumental defocusing had been made. The POD program, part of the popLA package (Los Alamos National Laboratory, Los Alamos, NM, USA), was used to plot the figures. Further details on the determination of the pole figure are described in ref 55.

The thermal behavior of the samples was investigated using the DSC Q20 Differential Scanning Calorimeter (TA Instruments) during heating from 20 to 280 °C (ABS/PET) and from 20 to 250 °C (PETG/PBT, PLA/PBT) at a rate of 10 °C min^{-1}. The samples were held at 280 °C (ABS/PET) or 250 °C (PETG/PBT, PLA/PBT) for 15 min after first heating.[56]

The TGA was performed from room temperature to 600 °C at 10 °C/min with a Rigaku Instrument Thermo Plus TG 8120 in a nitrogen atmosphere.

Solid-state NMR spectra were recorded on a Bruker AVANCE III WB 400 MHz spectrometer. The spinning rate for all experiments was 6 kHz. 13C cross-polarization magic-angle spinning spectra were obtained under two-pulse phase modulating proton decoupling. A recycle delay is 2 s. 1H spin−lattice relaxation time measurements both in the laboratory and in rotating frames T_1 and T_{1r} respectively were measured at room temperature by saturation recovery method and spin lock method, respectively.

Transmission electron microscopy (TEM) was performed using a Tesla BS 500 electron microscope at 90 kV. Samples were prepared as thin sections approximately 60 nm thick using an ultramicrotome (PowerTome PC, Boeckeler, USA) equipped with a 35° diamond knife (Diatome, Switzerland). No staining or any other chemical treatment was applied to sections prior to observation.

The mechanical properties of both untreated and HPT-processed blends were assessed using a tensile testing machine (Instron, Model 5582). Rectangular samples measuring 15 × 5 mm were prepared, with an initial clamp separation of 10 mm. A crosshead speed of 5%/min was applied, and each sample was tested five times under the same conditions. Modulus of elasticity, yield strength and yield stress were determined from the stress−strain curves of the samples. However, due to the small size of the HPT-processed specimens, it was not possible to measure the strain at break. The lack of a proper specimen shape resulted in stress concentrations at the clamping points, causing premature failure before sufficient elongation could occur.

■ ASSOCIATED CONTENT

Supporting Information

The Supporting Information is available free of charge at https://pubs.acs.org/doi/10.1021/acs.iecr.5c00328.

Figure S1: spin−lattice relaxation time measurements of ABS/PET initial and HPT processed blends to observe $T_{1\rho}$ decay curves for CH_2 of PET (red colored) and methyne carbon of ABS (blue colored) in (a) initial blend, (b) 1 GPa/γ = 440/1 rpm, (c) 1 GPa/ γ = 440/5 rpm, (d) 1 GPa/γ = 2200/1 rpm, (e) 1 GPa/γ = 2200/5 rpm, (f) 1 GPa/γ = 4400/1 rpm, (g) 1 GPa/γ = 4400/5 rpm, (h) 2 GPa/γ = 440/5 rpm, (k) 2 GPa/γ = 720/5 rpm, (l) 3 GPa/γ=440/5 rpm, (m) 3 GPa/γ = 720/5 rpm, (n) 1 GPa/γ = 440/3 rpm, (o) 1 GPa/γ = 2200/3 rpm, (p) 1 GPa/γ = 4400/3 rpm, (q) 1 GPa/γ = 440/7 rpm, (r) 1 GPa/γ = 2200/7 rpm, (s) 1 GPa/γ = 4400/7 rpm; Figure S2: spin−lattice relaxation time measurements of PET/ABS initial and HPT processed blends to

https://doi.org/10.1021/acs.iecr.5c00328
Ind. Eng. Chem. Res. 2025, 64, 7739−7750

observe $T_{1\rho}$ decay curves for CH_2 of PET (red colored) and methyne carbon of ABS (blue colored) in (a) initial blend, (b) 1 GPa/γ = 440/1 rpm, (c) 1 GPa/γ = 440/5 rpm, (d) 1 GPa/γ = 2200/1 rpm, (e) 1 GPa/γ = 2200/5 rpm, (f) 1 GPa/γ = 4400/1 rpm, (g) 1 GPa/γ = 4400/5 rpm, (h) 2 GPa/γ = 440/5 rpm, (k) 2 GPa/γ = 720/5 rpm, (l) 3 GPa/γ = 440/5 rpm, (m) 3 GPa/γ = 720/5 rpm, (n) 1 GPa/γ = 440/3 rpm, (o) 1 GPa/γ = 2200/3 rpm, (p) 1 GPa/γ = 4400/3 rpm, (q) 1 GPa/γ = 440/7 rpm, (r) 1 GPa/γ = 2200/7 rpm, (s) 1 GPa/γ = 4400/7 rpm; Figure S3: DSC and TGA thermograms of HPT-processed ABS/PET blends under 2 and 3 GPa, displaying the first heating (solid lines) and second heating/annealing (dashed lines); Figure S4: DSC and TGA thermograms of PETG/PBT and PLA/PBT blends; Figure S5: spin−lattice relaxation time measurements of initial and HPT- processed PLA/PBT (a−d) and PET-G/PBT (e−h) systems: the observed T1 recovery and $T_{1\rho}$ decay curves measured for CH_2 of PBT (red) and $-CH_3$ of PLA (blue) in (a, c) initial and (b, d) HPT-processed PLA/PBT systems and the observed T_1 recovery and $T_{1\rho}$ decay curves measured for PAR bonding carbon of PBT (red) and CH_2 of PET-G (blue) in (e, g) initial and (f, h) HPT-processed PET-G/PBT systems, asterisks (*) and (**) denote HPT processing at 2 and 3 GPa, respectively; Figure S6: normalized pole figures of the (110) crystallographic plane determined for initial and HPT processes blends (γ = 2200, 5 rpm, 1 GPa); Figure S7: DSC thermograms of HPT-processed PLA/PBT and PETG/PBT blends: effect of heating HPT-processed samples above the melting temperatures (230 °C for PETG/PBT and PLA/PBT) on crystallization behavior specifically the crystallization temperature; Figure S8: X-ray diffraction patterns of the studied blends as a function of pressure, accumulated shear strain (γ) and torsion speed: the effect of torsion speed is negligible, resulting in overlapping curves (a magnified view of this overlap is shown in the inset); Figure S9: exemplary of the respective stress−strain dependencies determined during uniaxial tensile test on initial (nonprocessed) and HPT processed blends (PDF)

AUTHOR INFORMATION

Corresponding Author

Iurii Vozniak − *Centre of Molecular and Macromolecular Studies, Polish Academy of Sciences, Lodz 90-363, Poland;* orcid.org/0000-0002-8123-0689; Email: wozniak@cbmm.lodz.pl

Authors

Roman Kulagin − *Karlsruhe Institute of Technology, Institute of Nanotechnology, Eggenstein-Leopoldshafen 76344, Germany*

Victor Beloshenko − *Donetsk Institute for Physics and Engineering named after O.O. Galkin, National Academy of Sciences of Ukraine, Kyiv 03028, Ukraine*

Ramin Hosseinnezhad − *Centre of Molecular and Macromolecular Studies, Polish Academy of Sciences, Lodz 90-363, Poland*

Artur Rozanski − *Centre of Molecular and Macromolecular Studies, Polish Academy of Sciences, Lodz 90-363, Poland;* orcid.org/0000-0001-7545-6246

Andrzej Galeski − *Centre of Molecular and Macromolecular Studies, Polish Academy of Sciences, Lodz 90-363, Poland;* orcid.org/0000-0003-3058-1312

Salim-Ramy Merouani − *Centre of Molecular and Macromolecular Studies, Polish Academy of Sciences, Lodz 90-363, Poland; The Bio-Med-Chem Doctoral School of the University of Lodz and Lodz Institutes of the Polish Academy of Sciences, Lodz 90-237, Poland*

Bogdan Savchenko − *Kyiv National University of Technologies and Design, Kyiv 01011, Ukraine*

Complete contact information is available at: https://pubs.acs.org/10.1021/acs.iecr.5c00328

Author Contributions

I.V.: conceptualization, methodology, validation, formal analysis, investigation, resources, data curation, writing-original draft, supervision, project administration. R.K.: conceptualization, methodology, validation, formal analysis, investigation, data curation, writing-review and editing. V.B.: methodology, formal analysis, writing-review and editing. R.H.: methodology, formal analysis, investigation, resources, visualization, writing-review and editing. A.R.: methodology, formal analysis, investigation, writing-review and editing. A.G.: methodology, formal analysis, writing-review and editing. S.R.M.: methodology, formal analysis, investigation, writing-review and editing. B.S.: methodology, formal analysis, investigation, writing-review and editing.

Notes

The authors declare no competing financial interest.

ACKNOWLEDGMENTS

This research was funded in part by the National Science Centre (Poland) under grant 2021/43/B/ST8/01443.

ABBREVIATIONS

HPT high-pressure torsion

REFERENCES

(1) Koning, C.; van Duin, M. M.; Pagnouille, C.; Jerome, R. Strategies for Compatibilization of Polymer Blends. *Prog. Polym. Sci.* **1998**, *23*, 707−757.

(2) Xu, Y.; Loi, J.; Delgado, P.; Topolkaraev, V.; McEneany, R. J.; Macosko, C. W.; Hillmyer, M. A. Reactive Compatibilization of Polylactide/Polypropylene Blends. *Ind. Eng. Chem. Res.* **2015**, *54*, 6108−6114.

(3) Brown, S. B. Reactive Compatibilization. In *Polymer Blends Handbook*, Utracki, L. A.; Wilkie, C. A., Eds.; Kluwer Academic Publishers: Dordrecht, 2003; pp. 517−676.

(4) Sonnier, R.; Taguet, A.; Rouif, S. Modification of Polymer Blends by E-Beam and Gamma-Irradiation. In *Functional Polymer Blends*, Mital, V., Eds.; CRC Press: Boca Raton, 2012; pp. 261−304.

(5) Rusa, C. C.; Wei, M.; Shuai, X.; Bullions, T. A.; Wang, X.; Rusa, M.; Uyar, T.; Tonelli, A. E. Molecular Mixing of Incompatible Polymers through Formation and Coalescence from Their Common Crystalline Cyclodextrin Inclusion Compounds. *J. Polym. Sci., Part B: Polym. Phys.* **2004**, *42*, 4207−4224.

(6) Kietzke, T.; Neher, D.; Landfester, K.; Montenegro, R.; Güntner, R.; Scherf, U. Novel Approaches to Polymer Blends Based on Polymer Nanoparticles. *Nat. Mater.* **2003**, *2*, 408−412.

(7) Taguet, A.; Cassagnaub, P.; Lopez-Cuesta, J.-M. Structuration, Selective Dispersion, and Compatibilizing Effect of (Nano)Fillers in Polymer Blends. *Prog. Polym. Sci.* **2014**, *39*, 1526−1563.

(8) Kim, D. Y.; Lee, J. B.; Lee, D. Y. Selective Localization of Nanofiller on Mechanical Properties of Poly(Lactic Acid)/Poly-

(Butylene Adipate-Co-Terephthalate) Nanocomposites via the Surface Energy and Melt Blending Technique. *Macromolecules* **2022**, *55*, 3287−3300.
(9) Seyedi, M.; Savchak, M.; Tiiara, A.; Luzinov, I. Toward Mechanical Recycling of Polystyrene/Polypropylene Blends with Bottlebrush-Modified Graphene Oxide as a Compatibilizer. *ACS Appl. Mater. Interfaces* **2022**, *14*, 35074−35086.
(10) Wang, H.; Dong, W.; Li, Y. Compatibilization of Immiscible Polymer Blends Using In Situ Formed Janus Nanomicelles by Reactive Blending. *ACS Macro Lett.* **2015**, *4*, 1398−1403.
(11) Kim, J.; Gray, M. K.; Zhou, H.; Nguyen, S. T.; Torkelson, J. M. Polymer Blend Compatibilization by Gradient Copolymer Addition during Melt Processing: Stabilization of Dispersed Phase to Static Coarsening. *Macromolecules* **2005**, *38*, 1037−1040.
(12) Park, T.; Zimmerman, S. C. Formation of a Miscible Supramolecular Polymer Blend through Self-Assembly Mediated by a Quadruply Hydrogen-Bonded Heterocomplex. *J. Am. Chem. Soc.* **2006**, *128*, 11582−11590.
(13) Sheiko, S. S.; Zhou, J.; Arnold, J.; Neugebauer, D.; Matyjaszewski, K.; Tsitsilianis, C.; Tsukruk, V. V.; Carrillo, J.-M. Y.; Dobrynin, A. V.; Rubinstein, M. Perfect Mixing of Immiscible Macromolecules at Fluid Interfaces. *Nat. Mater.* **2013**, *12*, 735−740.
(14) Pan, C.; Sugiyasu, K.; Takeuchi, M. Blending Conjugated Polymers without Phase Separation for Fluorescent Colour Tuning of Polymeric Materials through FRET. *Chem. Commun.* **2014**, *50*, 11814−11817.
(15) Picciani, P. H. S.; Medeiros, E. S.; Pan, Z.; Wood, D. F.; Orts, W. J.; Mattoso, L. H. C.; Soares, B. G. Electrical, Mechanical, and Thermal Properties of Electrospun Poly(Lactic Acid)/Polyaniline Blend Fibers. *Macromol. Mater. Eng.* **2010**, *295*, 618−627.
(16) Uemura, T.; Kaseda, T.; Sasaki, Y.; Inukai, M.; Toriyama, T.; Takahara, A.; Jinnai, H.; Kitagawa, S. Mixing of Immiscible Polymers Using Nanoporous Coordination Templates. *Nat. Commun.* **2015**, *6*, 7473.
(17) Coubrough, H. M.; Reynolds, M.; Goodchild, J. A.; Connell, S. D. A.; Mattsson, J.; Wilson, A. J. Assembly of Miscible Supramolecular Network Blends Using DDA·AAD Hydrogen-Bonding Interactions of Pendant Side-Chains. *Polym. Chem.* **2020**, *11*, 3593−3604.
(18) Martin, R.; Rekondo, A.; Ruiz de Luzuriaga, A.; Santamaria, A.; Odriozola, I. Mixing the Immiscible: Blends of Dynamic Polymer Networks. *RSC Adv.* **2015**, *5*, 17514.
(19) Furgiuele, N.; Lebovitz, A. H.; Khait, K.; Torkelson, J. M. Novel Strategy for Polymer Blend Compatibilization: Solid-State Shear Pulverization. *Macromolecules* **2000**, *33*, 225−228.
(20) Maris, J.; Bourdon, S.; Brossard, J.-M.; Cauret, L.; Fontaine, L.; Montembault, V. Mechanical Recycling: Compatibilization of Mixed Thermoplastic Wastes. *Polym. Degrad. Stab.* **2018**, *147*, 245−266.
(21) Will, T. A.; Lu, Y.; Wakabayashi, K. Effects of Polymer Properties on Solid-State Shear Pulverization: Thermoplastic Processability and Nanofiller Dispersibility. *ACS Appl. Polym. Mater.* **2023**, *5*, 1848−1858.
(22) Liu, R. Y. F.; Ranade, A. P.; Wang, H. P.; Bernal-Lara, T. E.; Hiltner, A.; Baer, E. Forced Assembly of Polymer Nanolayers Thinner than the Interphase. *Macromolecules* **2005**, *38*, 10721−10727.
(23) Moon, D.; Migler, K. B. Forced Assembly and Mixing of Melts via Planar Polymer Micro-Mixing. *Polymer* **2010**, *51*, 3147−3155.
(24) Perilla, J. E.; Jana, S. C. Coalescence of Immiscible Polymer Blends in Chaotic Mixers. *AichE J.* **2005**, *51*, 2675−2685.
(25) Gumerov, R. A.; Rumyantsev, A. M.; Rudov, A.; Pich, A.; Richtering, W.; Möller, M.; Potemkin, I. I. Mixing of Two Immiscible Liquids within the Polymer Microgel Adsorbed at Their Interface. *ACS Macro Lett.* **2016**, *5*, 612−616.
(26) Bai, L.; Huan, S.; Zhao, B.; Zhu, Y.; Esquena, J.; Chen, F.; Gao, G.; Zussman, E.; Chu, G.; Rojas, O. J. All-Aqueous Liquid Crystal Nanocellulose Emulsions with Permeable Interfacial Assembly. *ACS Nano* **2020**, *14*, 13380−13390.
(27) Pracella, M. Blends and Alloys. In *Modification of Polymer Properties*; Jasso-Gastinel, C. F.; Kenny, J. M., Ed.; Elsevier: 2017, pp. 155−184.
(28) Zhou, T.; Ning, X.; Wu, Z.; Lan, X.; Xu, C. Understanding the Interfacial and Self-Assembly Behavior of Multiblock Copolymers for Developing Compatibilizers Toward Mechanical Recycling of Polymer Blends. *Ind. Eng. Chem. Res.* **2024**, *63*, 6766−6773.
(29) Odunuga, S.; Li, Y.; Krasnochtchekov, P.; Bellon, P.; Averback, R. S. Forced Chemical Mixing in Alloys Driven by Plastic Deformation. *Phys. Rev. Lett.* **2005**, *95*, 045901.
(30) Arshad, S. N.; Lach, T. G.; Pouryazdan, M.; Hahn, H.; Bellon, P.; Dillon, S. J.; Averback, R. S. Dependence of Shear-Induced Mixing on Length Scale. *Scr. Mater.* **2013**, *68*, 215−218.
(31) Kormout, K. S.; Pippan, R.; Bachmaier, A. Deformation-Induced Supersaturation in Immiscible Material Systems During High-Pressure Torsion. *Adv. Eng. Mater.* **2017**, *19*, 1600675.
(32) Castro, M. M.; Montoro, L. A.; Isaac, A.; Kawasaki, M.; Figueiredo, R. B. Mechanical Mixing of Mg and Zn Using High-Pressure Torsion. *J. Alloy. Compd.* **2021**, *869*, 159302.
(33) Beygelzimer, Y.; Estrin, Y.; Mazilkind, A.; Scherere, T.; Baretzky, B.; Hahn, H.; Kulagin, R. Quantifying Solid-State Mechanical Mixing by High-Pressure Torsion. *J. Alloys Compd.* **2021**, *878*, 160419.
(34) Suryanarayana, C. Mechanical Alloying and Milling. *Prog. Mater. Sci.* **2001**, *46*, 1−184.
(35) Zhilyaev, A. P.; Langdon, T. G. Using High-Pressure Torsion for Metal Processing: Fundamentals and Applications. *Prog. Mater. Sci* **2008**, *53*, 893−979.
(36) Sauvage, X.; Chbihi, A.; Quelennec, X. Severe Plastic Deformation and Phase Transformations. *J. Phys.: Conf. Ser.* **2010**, *240*, 012003.
(37) Straumal, B.; Korneva, A.; Zięba, P. Phase Transitions in Metallic Alloys Driven by High Pressure Torsion. *Arch. Civ. Mech. Eng.* **2014**, *14*, 242−249.
(38) Korznikov, A. V.; Tram, G.; Dimitrov, O.; Korznikova, G. F.; Idrisova, S. R.; Pakiela, Z. The Mechanism of Nanocrystalline Structure Formation in Ni_3Al During Severe Plastic Deformation. *Acta Mater.* **2001**, *49*, 663−671.
(39) Prokoshkin, S. D.; Khmelevskaya, I. Y.; Dobatkin, S. V.; Trubitsyna, I. B.; Tatyanin, E. V.; Stolyarov, V. V.; Prokofiev, E. A. Alloy Composition, Deformation Temperature, Pressure, and Post-Deformation Annealing Effects in Severely Deformed Ti−Ni Based Shape Memory Alloys. *Acta Mater.* **2005**, *53*, 2703−2714.
(40) Kovács, Z.; Henits, P.; Zhilyaev, A. P.; Révész, Á. Deformation-Induced Primary Crystallization in a Thermally Non-Primary Crystallizing Amorphous $Al_{85}Ce_8Ni_5Co_2$ Alloy. *Scr. Mater.* **2006**, *54*, 1733−1737.
(41) Zhorin, V. A.; Kissin, Y. V.; Luizo, Y. V.; Fridman, N. M.; Yenikolopyan, N. S. Structural Changes in Polyolefins Due to the Combination of High Pressure and Shear Deformation. *Polym. Sci. U.S.S.R.* **1976**, *18*, 3057−3061.
(42) Zhorin, V. A.; Mironov, N. A.; Nikol'skii, V. G.; Yenikolopyan, N. S. Homogenization of Polyolefin Mixtures in Shear Deformation. *Polym. Sci. U.S.S.R.* **1980**, *22*, 440−447.
(43) Zhorin, V. A.; Kulakov, V. V.; Mironov, N. A.; Nikol'skii, V. G.; Chebotarevskii, A. E.; Yenikolopyan, N. S. Homogenization of Blends of Polypropylene and Ethylene-Propylene Rubber Under Shear in the Presence of Inorganic Fillers. *Polym. Sci. U.S.S.R.* **1982**, *24*, 1081−1084.
(44) Drazin, P. G.; Reid, W. H. *Hydrodynamic Stability*; Cambridge University Press: Cambridge, U.K, 2004.
(45) Lodge, T. P.; McLeish, T. C. B. Self-Concentrations and Effective Glass Transition Temperatures in Polymer Blends. *Macromolecules* **2000**, *33*, 5278−5284.
(46) Kozlov, G. V.; Beloshenko, V. A.; Lipskaya, V. O. The Relationship Between the Disorder Parameter and the Structure and Properties of Network Polymers. *Ukr. J. Phys.* **1996**, *41*, 222−225.
(47) Kozlov, G. V.; Novikov, V. U. A Cluster Model for the Polymer Amorphous State. *Phys.-Uspekhi* **2001**, *44*, 681−724.
(48) Kozlov, G. V.; Zaikov, G. E.; Lipatov, Y. S. The Structural Treatment of Fluctuation Free Vol. in the Amorphous State of Polymers. In *Chemical and Biological Kinetics New Horizons: vol. 1:*

https://doi.org/10.1021/acs.iecr.5c00328
Ind. Eng. Chem. Res. 2025, 64, 7739−7750

Chemical Kinetics, Zaikov, G. E., Eds.; CRC Press: Boca Raton, FL, 2005; pp. 484−516.
(49) Flory, P. Spatial Configuration of Macromolecular Chains. *Br. Polymer J.* **1976**, *8*, 1−10.
(50) Flory, P. Conformations of Macromolecules in Condensed Phase. *J. Pure Appl. Chem.* **1984**, *56*, 305−312.
(51) Edalati, K.; Horita, Z. A Review on High-Pressure Torsion (HPT) from 1935 to 1988. *Mater. Sci. Eng., A* **2016**, *652*, 325−352.
(52) Edalati, K. Metallurgical Alchemy by Ultra-Severe Plastic Deformation via High-Pressure Torsion Process. *Mater. Trans.* **2019**, *60*, 1221−1229.
(53) Vozniak, I.; Beloshenko, V.; Vozniak, A.; Zaïri, F.; Galeski, A.; Rozanski, A. Interfaces Generation via Severe Plastic Deformation − A New Way to Multiple Shape Memory Polymer Composites. *Polymer* **2023**, *267*, 125653.
(54) Alexander, L. E. *X-Ray Diffraction Methods in Polymer Science*; Wiley-Interscience: New York, NY, 1969.
(55) Slusarczyk, C.; Sieradzka, M.; Fabia, J.; Fryczkowski, R. Supermolecular Structure of Poly(butylene Terephthalate) Fibers Formed with the Addition of Reduced Graphene Oxide. *Polymers* **2020**, *12*, 1456.
(56) Galeski, A.; Bartczak, Z.; Argon, A. S.; Cohen, R. E. Morphological Alterations During Texture-Producing Plastic Plane-Strain Compression of High-Density Polyethylene. *Macromolecules* **1992**, *25*, 5705−5718.

https://doi.org/10.1021/acs.iecr.5c00328
Ind. Eng. Chem. Res. 2025, 64, 7739−7750